Characterizing Coherent Wind Structures using Large-Scale Particle Tracking Velocimetry: A Proof-of-Principle Study

G A Rosi[1], B la Bastide[1], J Gaebler[1,2], M Kinzel[3], and D E Rival[1]

[1]Department of Mechanical Engineering, University of Calgary, 2500 University Dr. NW, Calgary, Canada. [2]Department of Mechanical Engineering, Technische Universitaet Berlin, 135 Strasse des 17. Juni, Berlin, Germany. [3]GALCIT, California Institute of Technology, 1200 E California Blvd., Pasadena, USA

E-mail: garosi@ucalgary.ca

Abstract. The following study proposes a two-dimensional large-scale particle tracking velocimetry (LS-PTV) system to characterize coherent wind structures. Seven minutes of LS-PTV data is collected via an apparatus that seeds fog-filled soap bubbles into the wind at a height of 6m from the ground. The LS-PTV data is compared to 20 minutes of data collected concurrently from a wind mast at the same site. The LS-PTV system recorded a mean streamwise velocity of 1.35m/s with a standard deviation of 0.23m/s at a mean height of 2.50m with a standard deviation of 0.7m, which agrees well with the velocity profile measured by the wind mast. Furthermore, the Reynolds stresses measured by the LS-PTV system are found to compare to those measured by the wind mast and by Klebanoff [1] for a canonical turbulent boundary layer. The current study assumes that the centre-of-curvature trajectories of the particle pathlines are representative of the trajectories followed by the spanwise vortices. As a proof-of-principle study, this work has been successful in accurately describing the vortex distribution very near to the ground. However, the trajectories followed by the centres-of-curvature belonging to pathlines concurrently passing through the field-of-view were sporadic and uncorrelated.

1 Introduction

A clear characterization of extreme wind events remains elusive in the wind-engineering community. Traditionally, studies have quantified the occurrence frequency of extreme events in order to characterize the probability of their occurrence; see Kants et al. [2], Waechter et al. [3] and Kristensen et al. [4]. However, quantifying the likelihood of extreme events does not permit one to predict their future occurrence from wind-mast measurements, as this would require insight into the flow structure inherent of extreme events. Thus, recent studies have tried to identify extreme events within data sets via conditional analysis and then average their time traces to generate a mean extreme-event model; see Sterling et al. [5], Scarabino et al. [6], and Hansen and Larsen [7]. With conditional-analysis studies, however, it is not uncommon for resultant extreme-event models to vary greatly from study to study since the models are biased by the conditions employed to identify extreme events.

A more effective approach than the statistical methods described above would be to study the fundamental coherent motions (i.e. coherent structures,) that are ubiquitous to wind flows.

Coherent wind structures could be related to the coinciding wind turbulence and subsequently to the occurrence of extreme events. This approach has led to a substantially improved understanding of the mechanics of canonical turbulent boundary layers (TBLs) and the role that coherent structures play within canonical TBLs. Specifically, the hairpin vortex (see Robinson [8]) has been shown to be a ubiquitous structure within canoncial TBLs and is responsible for certain trends observed in the Reynold-stress profiles (Acarlar and Smith [9]) and turbulent energy spectra (Hutchins et al. [10]), as well as for the generation of large extreme events within the flow (Adrian [11]).

Towards the development of more accurate, predictable and all-inclusive extreme-event models, and given the substantial ground made in turbulence through the investigation of coherent structures, there has been a shift in wind research towards understanding the fundamental flow structures that comprise extreme wind events. However, the insights into the coherent motions of canonical TBLs have been made possible from two-dimensional (Wu and Christensen [12], Adrian [11]) and three-dimensional (Shroeder et al. [13]) optical velocimetry techniques, which produce temporally and spatially resolved data throughout the entire measurement domain. In contrast, the identification of coherent structures using classical wind-measurement techniques (e.g. wind masts) must rely solely on the correlation of velocity fluctuations at a few points. This method has merit in identifying very-large streamwise motions (Hutchins et al. [10]), but is severely limited in identifying vortices (in Scarabino et al. [6], Rosi et al. [14]). Furthermore, typical optical velocimetry setups used in laboratory settings cannot achieve sufficiently large measurement domains necessary to study wind flows, making them unsuitable for characterizing coherent wind structures.

An intermediate between classical wind-measurement techniques and laboratory-setting optical velocimetry setups exists in the form of large-scale particle tracking velocimetry (LS-PTV). The method tracks the motions of particles with sizes on the order of centimetres within a volume on the order of metres, which in turn produces concurrent velocity measurements throughout the entire volume. The method also reconstructs the pathlines followed by the particles, thereby describing the flow field in a Lagrangian frame of reference. Volume illumination, as well as camera calibration and synchronization are usual challenges that are faced by LS-PTV. To overcome this, LS-PTV must usually employ elaborate setups that are specific to the test facility; see Sun and Zhang [15]; Machacek [16]; Bosbach et al. [17]. Given the complexity of the apparatuses used by the aforementioned studies, their setups are unsuitable for outdoor measurements. Outdoor measurements also introduce challenges such as obtaining a suitable power source, coping with uneven ground, lighting and precipitation. Such challenges must be accounted for when developing LS-PTV for wind measurements.

Towards the characterization of coherent structures in wind flow, the current investigation proposes a simple LS-PTV system that acquires two-dimensional wind measurements by tracking the motions of fog-filled soap bubbles. LS-PTV measurements are acquired concurrently with measurements taken from a nearby wind mast. To quantify the accuracy of the LS-PTV system in measuring wind flows, the mean flow and Reynold stresses as measured by the system are compared against wind-mast measurements as well as against values taken from literature. Finally, as a first attempt at characterizing vortical structures within wind flow, the authors track the centres-of-curvature of pathlines to approximate the locations of spanwise-vortex centres.

2 Experimental Methods

On August 1st 2012, LS-PTV footage was recorded over a seven-minute period while wind-velocity measurements were simultaneously recorded from a wind mast nearby. The experiment was performed on flat, rural university property. Two satellite images of the site with the mean-wind direction indicated are presented in Figure 1. Figure 1a shows the entire site while Figure 1b is a magnified view of the immediate vicinity surrounding the mast with several geographical

features labeled. The steepest change in elevation (indicated by point L on Figure 1b) is a 5m descent over a 10m horizontal representing a 30° slope.

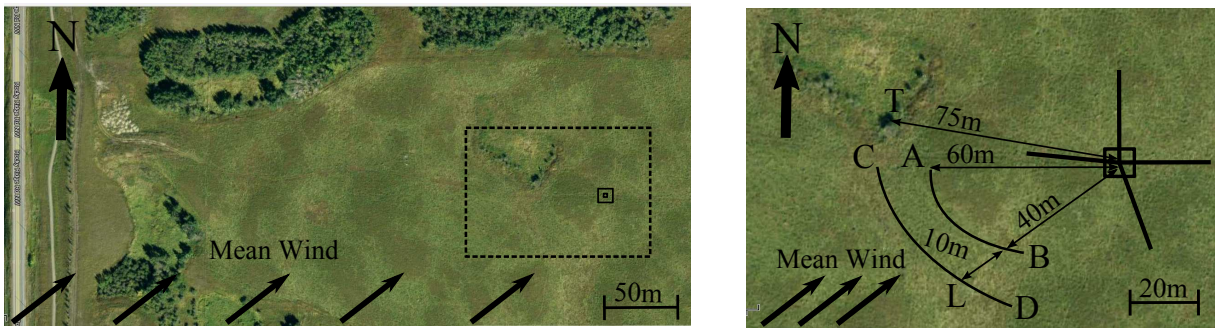

Figure 1: Satellite images of the LS-PTV test site. The scale is located in the bottom right of each image. (a) shows the entire site with the mast indicated by the double-square symbol contained in the dashed-line rectangle. The mean-wind direction is indicated as well. (b) is a magnified view of the area contained within the dashed-line rectangle. The mast is indicated by a square. The mast's guide wires are indicated by thick black lines and are approximately 30m in length. The area contained between line segments AB and CD indicates a small climb, which ascends from left to right. Point L indicates the lowest point in the gully which is 5m lower than the top of the climb. Point T indicates the position of the nearest tree to the mast. The images are taken from Google©Maps.

The wind mast with the approximate positioning of the sensors is depicted in Figure 2a, while a photograph of the mast with the surrounding landscape is shown in Figure 2b. The five cupped anemometers (CA) and wind vanes, as well as the two-component ultrasonic anemometer, provide ten-minute averages which describe the mean wind speed and direction. The two three-component ultrasonic anemometers (3CUS) at 40m and 50m heights quantify coherent structures as well as the Reynolds stresses in the wind. A schematic of the LS-PTV apparatus is provided in Figure 3. Fog-filled soap bubbles were created by modifying two commercial bubble guns to accept fog as an input rather than air. This method produced $30 - 40$mm diameter bubbles at a rate of 50 bubbles per second. The bubbles were seeded into the wind at a height of 6m. The field of view was located 30m downstream of the bubble generator to allow the particles to effectively disperse prior to reaching the field-of-view centre (point C in Figure 3). The camera was located at a spanwise distance of 12m from the field of view and at an angle of 12° with respect to the horizontal plane. The resulting field of view was elevated 1m above the ground, and captured an area that was 7m wide by 4m high. 13000 images were captured at a rate of 30Hz and at a resolution of 1280×720 pixels using a Nikon D7000 camera.

The current study assumes that the trajectories of spanwise-vortex centres are comparable to the trajectories followed by the centres-of-curvature of the particles tracked by the LS-PTV system. Consider a particle that moves at a velocity of $\vec{V} = u\hat{i} + v\hat{j}$ and that follows pathline P, as shown in Figure 4. When the particle is located at position $\vec{r} = x\hat{i} + y\hat{i}$, P exhibits a radius-of-curvature $\vec{R}$, whose magnitude equals $(u\dot{v} - v\dot{u})/(u^2 + v^2)^{3/2}$ (note dots indicate time derivatives). The particle's instantaneous direction is the unit vector of velocity $\hat{e_t}$, and $\vec{R}$ points along the unit vector normal to $\hat{e_t}$, which is prescribed to $\hat{e_n}$. The centre-of-curvature $\vec{C}$ is thereby located at the position $\vec{R} + \vec{r}$. Both $\vec{R}$ and $\vec{r}$ can be determined from the data collected by the LS-PTV system. Thus, the trajectories of the centres-of-curvature (hereafter referred to as centre trajectories) can be mapped. However, the centre trajectories may not always be representative of the trajectories followed by spanwise-vortex centres. Thus, the centre trajectories must meet

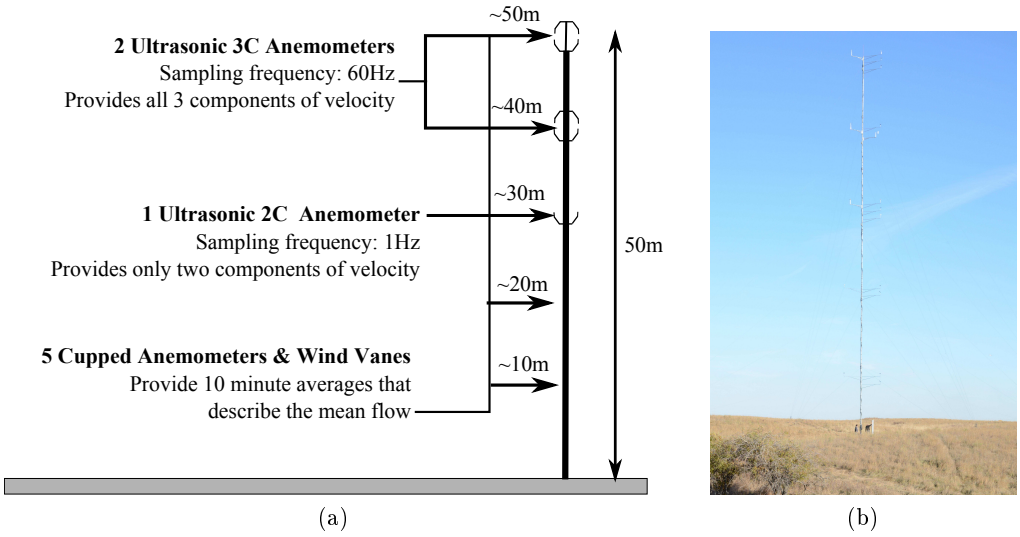

Figure 2: (a) A schematic of the wind mast with the approximate positioning of sensors indicated. (b) A photograph of the mast and surrounding terrain.

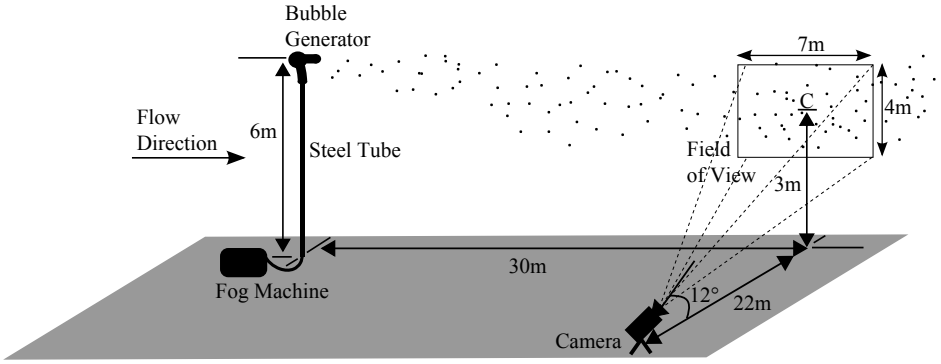

Figure 3: A schematic of the LS-PTV setup. The seeding apparatus is located on the left side, while the camera and its resultant field-of-view are located to the right.

the following two criteria. Firstly, it is unlikely that the PTV data can track vortices that fall far outside the field-of-view. Thus, only the portion of the centre trajectories that fall within a domain of $0\text{m} < x < 7\text{m}$ and a range of $0\text{m} < y < 10\text{m}$ will be considered. Secondly, vortices should neither rise nor fall rapidly but follow a relatively horizontal path. Thus, only the portions of the centre trajectories whose absolute slope is less than 60° will be considered. Note that the average height of the shallow-sloped portion of a centre trajectory is taken as the height of the trajectory's corresponding spanwise vortex.

3 Results

Figure 5a shows the mean velocities as recorded by the five cupped anemometers over the 20 minutes of data collection (hereupon referred to as the current data set). Also, the mean velocities derived from measurements taken by the cupped anemometers over 9 months for instances when the 50m cupped anemometer measured a velocity between 4m/s and 8m/s have been provided for comparison (hereupon referred to as the nine-month data set). Curves of the form $(u_*/k)\ln(y/y_0)$ have been fitted to the current data set as well as for the nine-month data set, where u_* is the friction velocity, k is the von Karman constant (approximately 0.4), y is the height from the ground and y_0 is friction length. From the curve fit, u_* and y_0 can be determined. For the current data set u_* and y_0 were found to be 0.37m/s and 0.21m, while for the nine-month data set u_* and y_0 were found to be 0.68m/s and 0.47m/s, respectively. Figure 5a also shows the mean streamwise velocity as recorded by the LS-PTV data, which was determined by averaging the

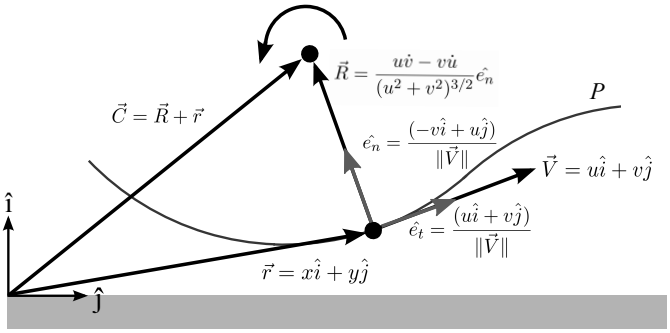

Figure 4: A tracked particle moving in the wind along path P. The particle and the centre-of-curvature of its path are shown. The position of the centre-of-curvature is given by $\vec{C} = \vec{R} + \vec{r}$, which can be determined by measurements taken by the LS-PTV system.

streamwise velocities and corresponding heights from the particle tracks. The mean velocity and mean height recorded by the LS-PTV data were found to be 1.35m/s and 2.50m, respectively, with standard deviations of 0.23m/s and 0.75m. The LS-PTV data's mean velocity falls within a standard deviation of the logarithmic-curve fit for the current data set suggesting that the LS-PTV system can accurately track the mean wind flow.

Figure 6 shows mean velocities measured by the cupped anemometers. Sensor height and velocity have been normalized by the the boundary layer thickness δ and freestream velocity U_0. A value of 1000m was assumed for δ. U_0 was determined by extrapolating the velocity at 1000m using the current data's mean-velocity profile shown in Figure 5a. U_0 was found to equal 7.12m/s. The black curve represents a normalized power-law fit suggested in Cheng [18] in which the fitting parameters are a function of y_0 and δ only. The good agreement between the sensor data and power-law fit suggests that 1000m is a good approximation for δ. Figure 6 also presents the normalized Reynolds stresses measured by the two 3CUS sensors at 0.04δ and 0.05δ and by the LS-PTV system at 0.0025δ. The Reynolds stresses for a canonical TBL measured by Klebanoff [1] are plotted for comparison. The normal stresses measured by the LS-PTV system and the 3CUS sensors are of the same order of magnitude, whereas the Reynolds stress measured by the LS-PTV system is nearly zero. The discrepancies are possibly due to the large discrepancy in Reynolds number. The data from Klebanoff [1] was collected at $Re_x = 4.2 \times 10^6$ while the current data set is approximately $Re_x = 1.3 \times 10^{10}$.

Figure 7 shows an instance of LS-PTV data typical of the current study's data set. Figure 7a plots the positions and velocities of some tracked bubbles during one snapshot in time, while Figure 7b shows the pathlines during a short interval of time. The centre trajectories are also shown on Figure 7b, and the portion of the trajectories with shallow slopes are indicated by red circles. As the trajectories enter the field-of-view's domain, the x-component of the trajectories seem to change in unison with the x-component of the pathline. The y-component fluctuates greatly between heights far from the field-of-view to heights within or just outside the field-of-view. Furthermore the slope of the trajectories tend to be more shallow at lower heights. The portions of the trajectories that exhibit large slopes are likely caused by portions of the pathlines that are roughly flat. It is observed that the centre trajectories exhibiting shallow slopes typically occur near or within the field-of-view and never above 10m. This would suggest that although the centre-of-curvature formulation may show promise in identifying spanwise vortices that pass within or near when they are near the field-of-view, it is not capable of identifying them beyond this height. Furthermore, the shallow-sloped segments belonging to centre trajectories that are concurrently passing through the field of view are typically short and uncorrelated. This further disputes the accuracy of the centre-of-curvature formulation in tracking spanwise

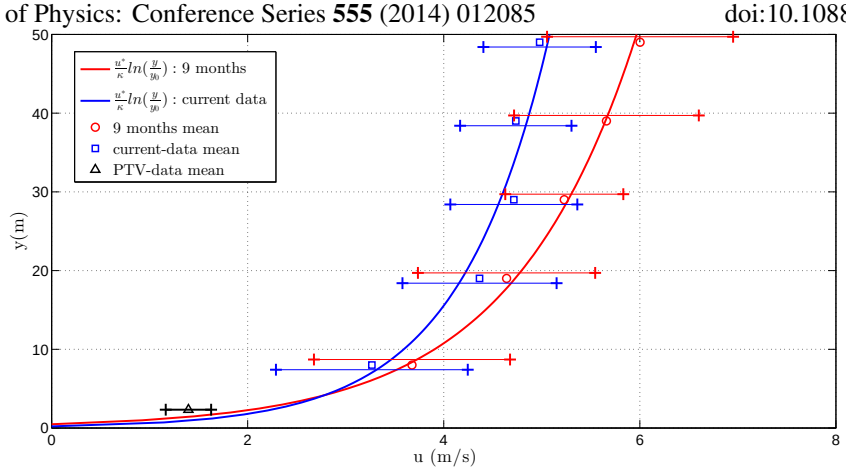

Figure 5: The mean velocity profiles measured by the cupped anemometers during the 20 minutes of data collection as well as over nine months when the 50m cupped anemometer recorded a velocity between 4m/s and 8m/s.

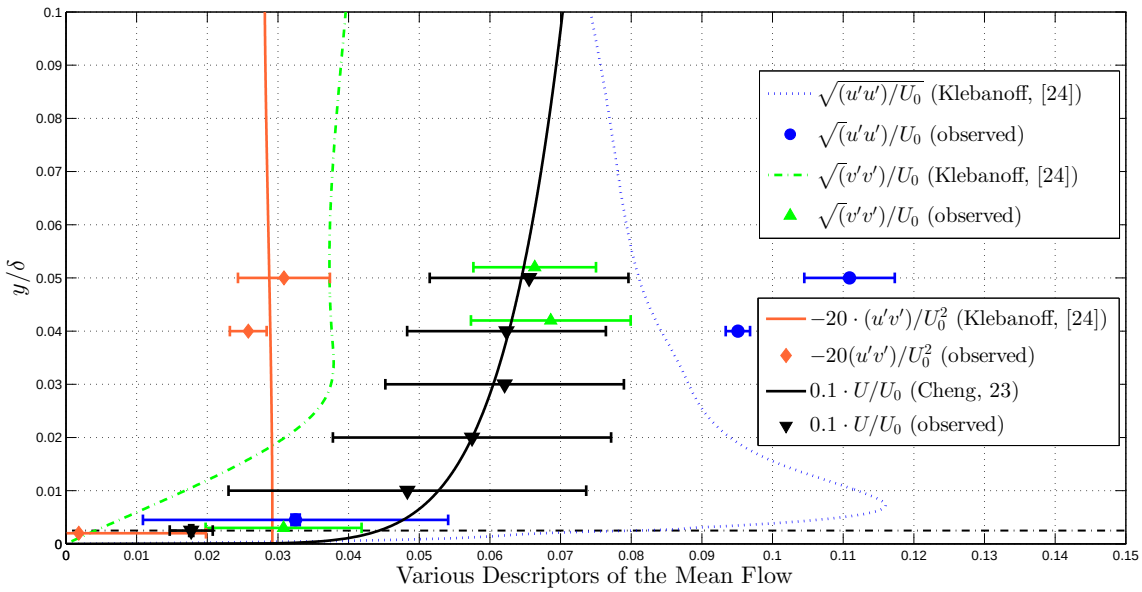

Figure 6: Canonical TBL and observed values of the mean velocity profile and Reynolds stresses. Note that all points were measured at 0.0025δ, 0.04δ or 0.05δ. However, some points have been displaced vertically to allow for visual representation. The solid error bars indicate the standard deviation. The dash-dot line indicates the mean height of the entire LS-PTV data set.

vortices. Firstly, the motion of a vortex should be continuous. Secondly if multiple particles are entrained in the same vortex, then their centre-of-curvatures should be well correlated if the centre-of-curvatures represents an appropriate approximation for the centre of a spanwise vortex.

Figure 8 shows the occurrence frequency of vortex centres with respect to normalized height, C/δ. The solid and hollow bars indicate the portions of the distribution that do and do not compare well with canonical-TBL studies. Spalart [19], Robinson [20] and Wu and Christensen [12] all observed that the distribution of vortex centres follows a Rayleigh distribution in height, which was also observed by the current study. However the aforementioned studies did not observe a drop in the occurrence frequency of spanwise vortices until heights well above 0.004δ, as observed in the current study. The quick drop of the occurrence frequency observed in the current study is likely caused by a bias introduced by the size and positioning of the field-of-view.

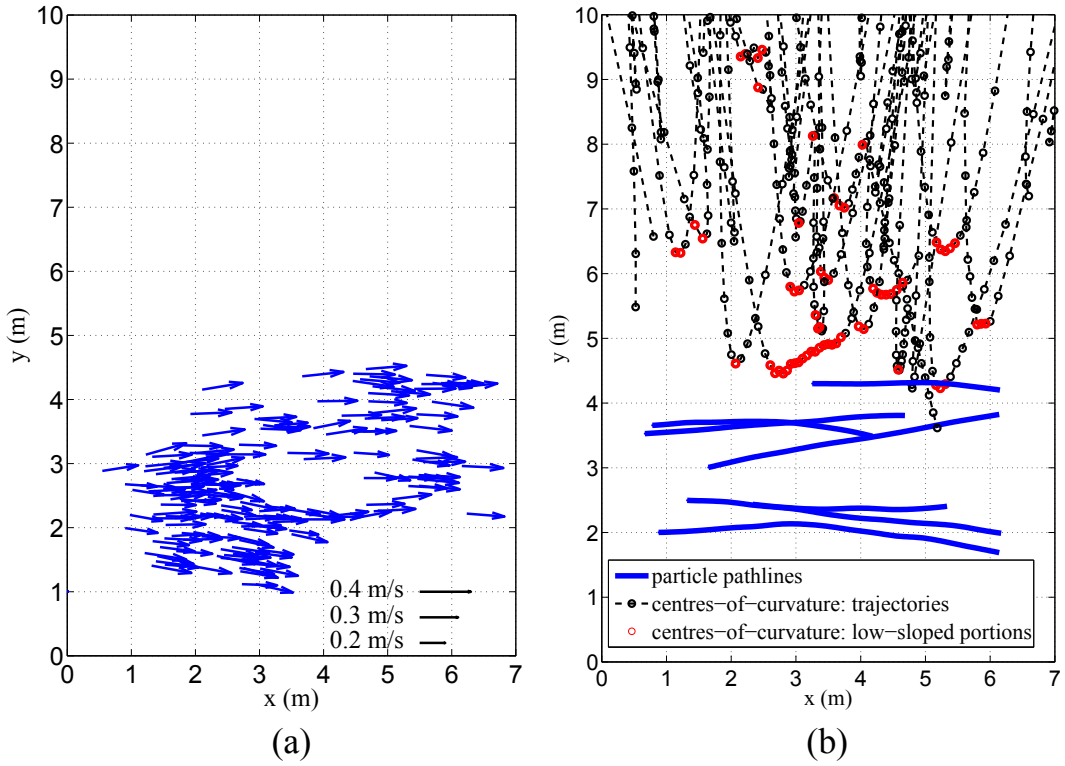

Figure 7: A typical instance of LS-PTV data. (a) shows some instantaneous bubble velocities while (b) shows the pathlines which started at that time frame. The lines which appear in the upper half of (b) are the centre trajectories of the pathlines. The circles indicate the portions of the trajectories whose absolute slope is shallow enough to meet the aforementioned criteria.

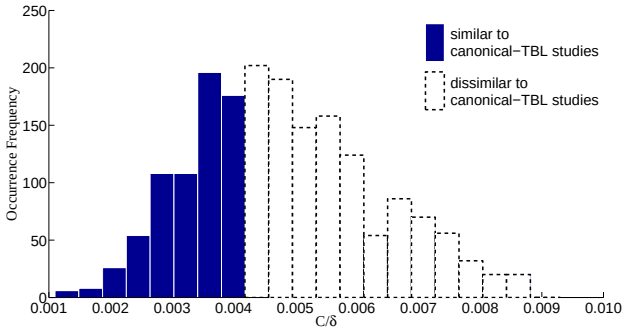

Figure 8: The occurrence distribution of curvature centres with respect to height.

4 Conclusions

A novel LS-PTV system, which tracks the motion of fog-filled soap bubbles to extract velocity measurements, has been proposed as a method to characterize wind flows and coherent structures in the atmospheric boundary layer. Data recorded using the LS-PTV system was compared to wind-mast data measured simultaneously at the same site. The mean velocity and Reynolds stresses as measured by the LS-PTV system agreed well with measurements taken by the wind mast, indicating the accuracy of the system in tracking wind flows. The system has been redeveloped to allow acquisition of three-dimensional velocity measurements. The reader is referred to Rosi et al. (online first) [21] for a more complete description and characterization of the system's capabilities.

As a first attempt at characterizing vortical structures in wind flows, the centres of spanwise vortices were approximated as the centres-of-curvatures of pathlines. The method resulted in occurrence-frequency distribution for vortex-centre height that agreed with canonical TBL studies. However, the trajectories of spanwise vortices mapped by the formulation were sporadic and uncorrelated. A more reliable method for tracking vortical structures remains to be developed. Ultimately, the identification of Lagrangian coherent structures (see Peacock and Haller [22]) will be achievable from the pathlines measured by the system. Currently, the authors are working towards increasing the seeding density within the field of view and by by scaling up.

References

[1] Klebanoff P 1955 *NACA Rep. 1110*

[2] Kants H, Holstein D, Ragwitz M and Vitanov N K 2004 *8th Experimental Chaos Conference* (American Institute of Physics)

[3] Wachter M, Holling M, Milan P and Peinke J 2011 *6th AIAA Theoretical Fluid Mechanics Conference* (American Institute of Aeronautics and Astronautics)

[4] Kristensen L, Casanova M, Courtney M S and Troen I 1991 *Boundary-Layer Meteorology* **55** 91–107

[5] Sterling M, Baker C J, Richards P J, Hoxey R P and Quinn A D 2006 *Wind and Structures* **9** 193–215

[6] Scarabino A, Sterling M, Richards P J, Baker C J and Hoxey R P 2007 *Wind and Structures* **10** 135–151

[7] Hansen K S and Larsen G C 2007 *The Science of Making Torque from Wind* 75 (IOP Publishing)

[8] Robinson S K 1991 *Annual Review of Fluid Mechanics* **23** 601–639

[9] Acarlar M S and Smith C R 1987 *Journal of Fluid Mechanics* **175** 43–83

[10] Hutchins N, Nickels T B, Marusic I and Chong M 2009 *Journal of Fluid Mechanics* **635** 103–136

[11] Adrian R J 2007 *Physics of Fluids* **19**

[12] Wu Y and Christensen K T 2006 *Journal of Fluid Mechanics* **568** 55–76

[13] Schroeder A, Geisler R, Staack K, Elsinga G E, Scarano F, Wieneke B, Henning A, Poelma C and Westerweel J 2011 *Experiments in Fluids* **50** 1071–1091

[14] Rosi G A, Martinuzzi R J and Rival D E 2013 *Journal of Wind Engineering and Industrial Aerodynamics* **119**

[15] Sun Y and Zhang Y 2003 *American Society of Heating, Refridgeration, Air-Conditioning Engineers* **09** 540–8

[16] Machacek M 2003 *A Quantitative Visualization Tool for Large Wind Tunnel Experiments* Ph.D. thesis Swiss Federal Institute of Technology

[17] Bosbach J, Kuhn M, Wagner C, Raffel M, Resagk C, du Puits R and Thess A 2006 *13th International Symposium on Applications of Laser Techniques to Fluid Mechanics*

[18] Cheng N S 2007 *Advances in Water Resources*

[19] Spalart P R 1986 *Journal of Fluid Mechanics* **187** 61–98

[20] Robinson S K 1989 *IUTAM Symposium on Structure of Turbulence and Drag Reduction* pp 23–50

[21] Rosi G A, Sherry M, Kinzel M and Rival D E 2014 *Experiments in Fluids*

[22] Peacock T and Haller G 2013 *Physics Today* **41** 1–7